

Three-Body Dynamics with Gravitational Wave Emission

Kayhan Gltekin

M. Coleman Miller

Douglas P. Hamilton

University of Maryland, College Park, Dept. of Astronomy

ABSTRACT

We present numerical three-body experiments that include the effects of gravitational radiation reaction by using equations of motion that include the 2.5-order post-Newtonian force terms, which are the leading order terms of energy loss from gravitational waves. We simulate binary-single interactions and show that close approach cross sections for three $1 M_{\odot}$ objects are unchanged from the purely Newtonian dynamics except for close approaches smaller than 10^{-5} times the initial semimajor axis of the binary. We also present cross sections for mergers resulting from gravitational radiation during three-body encounters for a range of binary semimajor axes and mass ratios including those of interest for intermediate-mass black holes (IMBHs). Building on previous work, we simulate sequences of high-mass-ratio three-body encounters that include the effects of gravitational radiation. The simulations show that the binaries merge with extremely high eccentricity such that when the gravitational waves are detectable by *LISA*, most of the binaries will have eccentricities $e > 0.9$ though all will have circularized by the time they are detectable by LIGO. We also investigate the implications for the formation and growth of IMBHs and find that the inclusion of gravitational waves during the encounter results in roughly half as many black holes ejected from the host cluster for each black hole accreted onto the growing IMBH.

Subject headings: stellar dynamics — gravitational waves — black hole physics — galaxies: star clusters — globular clusters: general — methods: n -body simulations

1. Introduction

With increasing evidence in support of the existence of intermediate-mass black holes (IMBHs), interest in these objects as gravitational wave sources is growing. With masses $\sim 10^2$ to $10^4 M_{\odot}$,

IMBHs are black holes that are more massive than stellar-mass black holes yet smaller than supermassive black holes found at the centers of galaxies. The primary motivation for IMBHs comes from observations of ultraluminous X-ray sources (ULXs): extragalactic, non-nuclear, point sources with inferred bolometric luminosities $L \gtrsim 3 \times 10^{39}$ erg s $^{-1}$ (see Miller & Colbert 2004 for a review). Such luminosities are greater than the Eddington luminosity of a $20 M_{\odot}$ object, which is the highest mass black hole that can be produced with roughly solar metallicity stellar evolution (Fryer & Kalogera 2001). The ULXs are thought to be powered by black holes because many are variable, but they cannot be powered by supermassive black holes or they would have sunk to the center of their host galaxies because of dynamical friction.

If, however, the intrinsic luminosity is much smaller than that inferred from the X-ray flux because the observed emission originates from a narrow beam directed towards us, then the lower limit on the mass can fall into stellar-mass black hole range (King et al. 2001). In such a case, these objects would be stellar-mass analogues of blazars. There is, however, evidence in support of quasi-isotropic emission from ULXs. First, recent observations of a $L_X \sim 10^{40}$ erg s $^{-1}$ ULX in the Holmberg II dwarf irregular galaxy show HeII emission from gas surrounding the ULX and line ratios in agreement with photoionization from a quasi-isotropically emitting X-ray source, thus giving weight to the picture that ULXs are more massive than stellar-mass black holes (Kaaret et al. 2004; Pakull & Mirioni 2001). Second, observations of ULX spectra that are fit with a combined power-law and multi-colored disk model indicate disk temperatures much lower than those found in known stellar-mass black hole X-ray binaries (Miller, Fabian, & Miller 2004). The temperature should scale as $T \sim M^{-1/4}$, and thus the inferred temperatures also favor a larger mass. Finally, Strohmayer & Mushotzky (2003) discovered a quasi-periodic oscillation (QPO) in the X-ray brightness of the brightest ULX in M82 (M82 X-1), whose X-ray luminosity is $L_X \approx 8 \times 10^{40}$ erg s $^{-1}$. The QPO, which has an rms amplitude of 8.5% at a centroid frequency of 54 mHz, is thought to come from the disk but is too strong to be consistent with a beamed source that is powered by a stellar-mass black hole. Thus there is strong evidence that at least some ULXs cannot be beamed stellar-mass X-ray binaries. There has also been theoretical work that suggests radiation-driven inhomogeneities can allow luminosities up to 10 times the Eddington limit (Begelman 2002; Ruszkowski & Begelman 2003), but the most luminous ULXs would still require a black hole more massive than stellar-mass black holes to power their bright, variable X-ray luminosity.

A key to understanding ULXs and IMBHs is their environment. ULXs are often found in starburst galaxies and in associations with stellar and globular clusters. For example, M82 X-1, one of the most promising IMBH candidates, is spatially coincident with the young stellar cluster MGG 11 as determined by near infrared observations (McCrady et al. 2003). Numerical simulations of MGG 11 show that due to its short dynamical friction timescale compared to the main sequence lifetime of the most massive stars, runaway growth by collisions between massive stars can cause a

star to grow to $\sim 3000 M_{\odot}$, after which it could evolve into an IMBH (Portegies Zwart et al. 2004). Fabbiano et al. (2001) found a spatial correlation of ULXs with stellar clusters in the merging Antennae system in excess of that expected from a uniform distribution of ULXs. A comparison of Chandra and HST images of the CD galaxy NGC 1399 at the center of the Fornax cluster shows a spatial correlation between many of its X-ray point sources and its globular clusters (Angelini et al. 2001). These X-ray point sources include two of the three sources with $L_X \gtrsim 2 \times 10^{39}$ erg s $^{-1}$, and the globular cluster and X-ray positions agree to within the combined astrometric uncertainties. In addition, evidence from radial velocities of individual stars in M15 as well as velocity and velocity dispersion measurements in G1 indicate that these globular clusters may harbor large dark masses in their cores ($\sim 3000 M_{\odot}$ and $1.7 (\pm 0.3) \times 10^4 M_{\odot}$, respectively, Gebhardt et al. 2000, 2002; Gerssen et al. 2002; Gebhardt et al. 2005). For M15 the data cannot rule out the absence of dark mass at the 3σ level, but the most recent observations of G1 can rule out the absence of dark mass at the 97% confidence level (Gebhardt et al. 2005). In both cases, the observations are of special interest because they are the only direct dynamical measurements of the mass of possible IMBHs. Finally, the Galactic globular cluster NGC 6752 contains two millisecond pulsars with high, negative spin derivatives in its core as well as two other millisecond pulsars well into the halo of the cluster at 3.3 and 1.4 times the half mass radius of the globular cluster (Colpi et al. 2003, 2002). The pulsars in the cluster core can be explained by a line-of-sight acceleration by $10^3 M_{\odot}$ of dark mass in the central 0.08 pc (Ferraro et al. 2003). While the pulsars in the outskirts of the cluster can be explained by exchange interactions with binary stars, the most likely explanation is that they were kicked from the core in a close interaction with an IMBH, either a single IMBH or a binary that contains an IMBH (Colpi et al. 2003, 2002).

One of the most intriguing questions regarding IMBHs is the method of their formation. They must form differently than stellar-mass black holes, which are the result of a core-collapse supernova and have a maximum mass of $20 M_{\odot}$, and they are distinct from supermassive black holes, which have masses $10^6 M_{\odot}$ to $10^9 M_{\odot}$ and are found at the centers of galaxies. Several studies have found that IMBHs may form in young stellar clusters where a core collapse leads to direct collisions of stars (Ebisuzaki et al. 2001; Gürkan et al. 2004; Portegies Zwart & McMillan 2002). Miller & Hamilton (2002b) proposed that IMBHs form from the mergers of stellar-mass black holes in a dense globular cluster, and Gültekin et al. (2004, hereafter Paper I) expanded this to include the mergers of stellar-mass black holes with the merger remnant of a young stellar cluster core collapse.

Of particular interest is the study of IMBHs as sources of detectable gravitational waves (Hopman & Portegies Zwart 2005; Matsubayashi et al. 2004; Miller 2002; Will 2004). Orbiting black holes are exciting candidates for detectable gravitational waves. At a distance d a mass m in

a Keplerian orbit of size r around a mass $M \gg m$ the gravitational wave amplitude is

$$h \sim \frac{G^2 M m}{c^4 r d} = 4.7 \times 10^{-25} \left(\frac{M}{M_\odot} \right) \left(\frac{m}{M_\odot} \right) \left(\frac{r}{\text{AU}} \right)^{-1} \left(\frac{d}{\text{kpc}} \right)^{-1}, \quad (1)$$

where G is the gravitational constant and c is the speed of light. For comparison, with one-year integrations the *Laser Interferometer Space Antenna (LISA)* and Advanced LIGO are expected to reach down to sensitivities of 10^{-23} at frequencies of 10 mHz and 100 Hz, respectively. Thus binaries containing IMBHs with $M \gtrsim 100 M_\odot$ with small separations at favorable distances are strong individual sources. During inspiral the frequency of gravitational waves increases as the orbit shrinks until it reaches the innermost stable circular orbit (ISCO) where the orbit plunges nearly radially towards coalescence. Because of the quadrupolar nature of gravitational waves, the gravitational wave frequency for circular binaries is twice the orbital frequency. At the ISCO for a non-spinning black hole with $M \gg m$, where $r_{\text{ISCO}} = 6GM/c^2$ and $h \sim Gm/6c^2d$ is independent of the mass of the primary, the gravitational wave frequency is

$$f_{\text{GW}} = 2f_{\text{orb}} = 2 \left(\frac{GM}{4\pi^2 r_{\text{ISCO}}^3} \right)^{1/2} \approx 4400 \text{ Hz} \left(\frac{M_\odot}{M} \right). \quad (2)$$

Thus a binary with a $100 M_\odot$ black hole will pass through *LISA* band (10^{-4} to 10^0 Hz Danzmann 2000) and into the bands of ground-based detectors such as LIGO, VIRGO, GEO-600, and TAMA (10^1 to 10^3 Hz, Fidecaro & VIRGO Collaboration 1997; Schilling 1998; Barish 2000; Ando & the TAMA collaboration 2002) whereas a $1000 M_\odot$ black hole will be detectable by *LISA* during inspiral but will not reach high enough frequencies to be detectable by currently planned ground-based detectors. After the final inspiral phase, the gravitational wave signal goes through a merger phase, in which the horizons cross, and a ringdown phase, in which the spacetime relaxes to a Kerr spacetime (Flanagan & Hughes 1998a,b; Cutler & Thorne 2002). The merger and ringdown phases emit gravitational waves at a higher frequency with a characteristic ringdown frequency of $f \sim 10^4 \text{ Hz} (M/M_\odot)^{-1}$ so that mergers with more massive IMBHs will still be detectable with ground-based detectors.

IMBHs in dense stellar systems are a unique source of gravitational waves. Through mass segregation, the most massive objects will sink to the center of a stellar cluster as dynamical interactions between objects tend towards equipartition of energy. For a cluster that is old enough to contain compact stellar remnants, the stellar-mass black holes, including those in binary systems, and IMBHs will congregate at the center and interact more frequently. For any reasonable mass function, the total mass of black holes in a cluster is large enough that mass segregation is a runaway process, known as the “mass stratification instability” (e.g., O’Leary et al. 2005). Through an exchange bias in which the most massive objects tend to end up with a companion after a three-body encounter, IMBHs will swap into binaries. Thus in a dense stellar system with an IMBH and massive binaries, the IMBH is likely to be found in the binary and to be a potential strong source

of gravitational waves. The IMBH-containing binary will continue to interact with objects in the cluster and to acquire ever more massive companions. In Paper I we found that a binary with an IMBH that undergoes repeated interactions in a stellar cluster will have a very high eccentricity after its last encounter before merging, and a significant fraction will retain a measurable eccentricity ($0.1 \lesssim e \lesssim 0.2$) when they are most easily detectable with *LISA* (see also O’Leary et al. 2005). Because detection of inspiral requires the comparison of the signal to a pre-computed waveform template that depends on the orbital properties of the binary, knowing the eccentricity distribution is useful. For $e \lesssim 0.2$, circular templates are accurate enough to detect the gravitational wave signal with LIGO (Martel & Poisson 1999), and this is likely to be the case for *LISA* as well.

If stellar clusters frequently host IMBHs, then currently planned gravitational wave detectors may detect mergers within a reasonable amount of time. Optimistic estimates put the upper limit to the Advanced LIGO detection rate of all black holes in dense stellar clusters at $\sim 10 \text{ yr}^{-1}$ (O’Leary et al. 2005). The *LISA* detection rate for 1 yr integration and signal-to-noise ratio of $\text{S/N} = 10$ is (Will 2004)

$$v_{\text{det}} \approx 10^{-6} \left(\frac{H_0}{70 \text{ km s}^{-1} \text{Mpc}^{-1}} \right)^3 \left(\frac{f_{\text{tot}}}{0.1} \right) \left(\frac{\mu}{10 M_{\odot}} \right)^{19/8} \left(\frac{M_{\text{max}}}{100 M_{\odot}} \right)^{13/4} \left(\ln \frac{M_{\text{max}}}{M_{\text{min}}} \right)^{-1} \text{yr}^{-1}, \quad (3)$$

where H_0 is the Hubble constant, f_{tot} is the total fraction of globular clusters that contain IMBHs, μ is the reduced mass of the merging binary, and M_{min} and M_{max} denote the range in masses of IMBHs in clusters. If we assume that $M_{\text{max}} = 10^3 M_{\odot}$, $\mu = 10 M_{\odot}$, $f_{\text{tot}} = 0.8$ (O’Leary et al. 2005), $H_0 = 70 \text{ km s}^{-1} \text{Mpc}^{-1}$, and $M_{\text{min}} = 10^2 M_{\odot}$, then we get a rate of 0.006 yr^{-1} . This, however, implies that $10^3 M_{\odot}$ black holes are continuously accreting $10 M_{\odot}$ black holes, which is unlikely to be the case. Since the distance out to which *LISA* can detect a given gravitational wave luminosity D_L scales as the square root of the integration time T , the volume probed scales as $V \sim D_L^3 \sim T^{3/2}$. This means that a 10 yr integration could yield a rate of 0.2 yr^{-1} , and if IMBHs with mass $M = 10^4 M_{\odot}$ are common, the rate could be much higher. These rates, however, are optimistic and should be considered as upper limits. A gravitational wave detection of an IMBH with high signal-to-noise could also yield the spin parameter and thus shed light on the formation mechanism of the IMBH (Miller 2002). A full understanding of the gravitational wave signals from IMBHs requires a more detailed study of the complicated dynamics and gravitational radiation of these systems.

In this paper we present a study of the dynamics of black holes in a stellar cluster using numerical simulations that include the effects of gravitational radiation. We include gravitational radiation reaction by adding a drag force to the Newtonian gravitational calculation. Our treatment is similar to that of Lee (1993), but we focus on individual encounters and sequences of encounters and the resulting mergers instead of ensemble properties of the host cluster. Paper I incorporated gravitational radiation by integrating the Peters (1964) orbit-averaged equations for orbital evo-

lution of a binary that is emitting gravitational waves, but in this paper we include the energy loss from gravitational radiation for arbitrary motion of the masses. Although the vast majority of three-body interactions do not differ greatly from a purely Newtonian simulation, an important few involve close approaches in which gravitational waves carry away a dynamically significant amount of energy such that it may cause the black holes to merge quickly in the middle of the encounter. This is qualitatively different from the mergers in Paper I which were caused by gravitational waves emitted by isolated binaries between encounters, and this new effect is important in considering detectable gravitational waves as well as IMBH growth.

In § 2 we describe our method of including gravitational waves as a drag force as well as numerical tests of its accuracy. We present our simulations and major results in § 3 and discuss the implications for IMBH formation and gravitational wave detection in § 4.

2. Numerical Method

The numerical method we use here is much the same as is described in § 2 of Paper I. In order to study the dynamics of a massive binary in a dense stellar environment, we simulate the encounters between the binary and single objects. We include both individual encounters and sequences of encounters, all of which include gravitational radiation emission. When simulating sequences, we allow the properties of the binary to evolve from interactions with singles, and we follow the binary until a merger occurs. A merger is determined to occur when the separation between the two masses is less than $G(m_0 + m_1)/c^2$. The simulations are run using the same code as in Paper I with a few exceptions. The integration engine is now HNDrag, which is an extension of HNBody (K. Rauch & D. Hamilton, in preparation)¹. Both HNBody and HNDrag can include the first-order post-Newtonian corrections responsible for pericenter precession based on the method of Newhall et al. (1983). HNDrag also has the ability to include pluggable modules that can add extra forces or perform separate calculations such as finding the minimum separation between all pairs of objects. In this paper we ignore the second-order post-Newtonian terms, which contribute higher-order corrections to the pericenter precession, and we include the effects of gravitational radiation on the dynamics of the particles through the addition of a force that arises from the 2.5-order post-Newtonian equation of motion for two point masses. The acceleration on a mass m_0 from gravitational waves emitted in orbit around a mass m_1 can be written as

$$\frac{d\mathbf{v}_0}{d\tau} = \frac{4G^2 m_0 m_1}{5c^5 r^3} \left[\hat{r}(\hat{r} \cdot \mathbf{v}) \left(-6\frac{Gm_0}{r} + \frac{52}{3}\frac{Gm_1}{r} + 3v^2 \right) + \mathbf{v} \left(2\frac{Gm_0}{r} - 8\frac{Gm_1}{r} - v^2 \right) \right] \quad (4)$$

¹See <http://janus.astro.umd.edu/HNBody/>.

where $\mathbf{r} = \mathbf{r}_1 - \mathbf{r}_0$ and $\mathbf{v} = \mathbf{v}_1 - \mathbf{v}_0$ are the relative position and velocity vectors between the two masses (Damour & Deruelle 1981; Damour 1982, 1983, for more recent treatments that use different techniques and arrive at the same result, see Itoh, Futamase, & Asada 2001 and Blanchet, Faye, & Ponsot 1998). Since Equation 4 introduces a momentum flux on the center of mass of the system, we partition the force so that it is equal and opposite and for reasons of computational efficiency to get an acceleration of

$$\frac{d\mathbf{v}_0}{dt} = \frac{4G^2}{5c^5} \frac{m_0 m_1}{r^3} \left(\frac{m_1}{m_0 + m_1} \right) \left[\hat{r} (\hat{r} \cdot \mathbf{v}) \left(\frac{34}{3} \frac{G(m_0 + m_1)}{r} + 6v^2 \right) + \mathbf{v} \left(-6 \frac{G(m_0 + m_1)}{r} - 2v^2 \right) \right]. \quad (5)$$

This expression is equivalent to Eq. 21 from Lee (1993). When orbit-averaged, Equation 5 gives the Peters (1964) equations for semimajor axis and eccentricity evolution:

$$\frac{da}{dt} = -\frac{64}{5} \frac{G^3 m_0 m_1 (m_0 + m_1)}{c^5 a^3 (1 - e^2)^{7/2}} \left(1 + \frac{73}{24} e^2 + \frac{37}{96} e^4 \right) \quad (6)$$

$$\frac{de}{dt} = -\frac{304}{15} \frac{G^3 m_0 m_1 (m_0 + m_1)}{c^5 a^4 (1 - e^2)^{5/2}} \left(e + \frac{121}{304} e^3 \right). \quad (7)$$

We tested the inclusion of this force in the integrator by comparison with direct, numerical integration of Equations 6 and 7 for two different binaries with masses $m_0 = m_1 = 10 M_\odot$ and initial semimajor axis $a_0 = 1$ AU: one with initial eccentricity $e_0 = 0$ and one with initial eccentricity $e_0 = 0.9$ (Fig. 1). The N -body integration of these binaries made use of HNDrag’s enhancement factor, which artificially augments the magnitude of the drag forces for the purposes of testing or simulating long-term effects. For this test and all numerical integrations with HNDrag, we used the fourth-order Runge-Kutta integrator. For both the circular and the high eccentricity cases, the N -body integrations agree very well with the Peters (1964) equations. Examination of Equation 5 reveals that even though physically the emission of gravitational radiation can only remove energy from the system, the equation implies $\dot{E} > 0$ for $\hat{r} \cdot \hat{v} > 0$ in hyperbolic orbits, becoming worse as the eccentricity increases (Lee 1993). Integration of Equation 5 over an entire orbit, however, does lead to the expected energy loss. This is because there is an excess of energy loss at pericenter, which cancels the energy added to the system (Lee 1993). Thus this formulation does not introduce significant error as long as the integration is calculated accurately at pericenter, which we achieve by setting HNDrag’s relative accuracy parameter to 10^{-13} , and the two objects are relatively isolated, which we discuss below.

We also tested the N -body integration with gravitational radiation for unbound orbits against the maximum periastron separation for two objects in an initially unbound orbit to become bound to each other (Quinlan & Shapiro 1989):

$$r_{p,\max} = \left(\frac{85\pi\sqrt{2}G^{7/2}m_0m_1(m_0 + m_1)^{3/2}}{12c^5v_\infty^2} \right)^{2/7}, \quad (8)$$

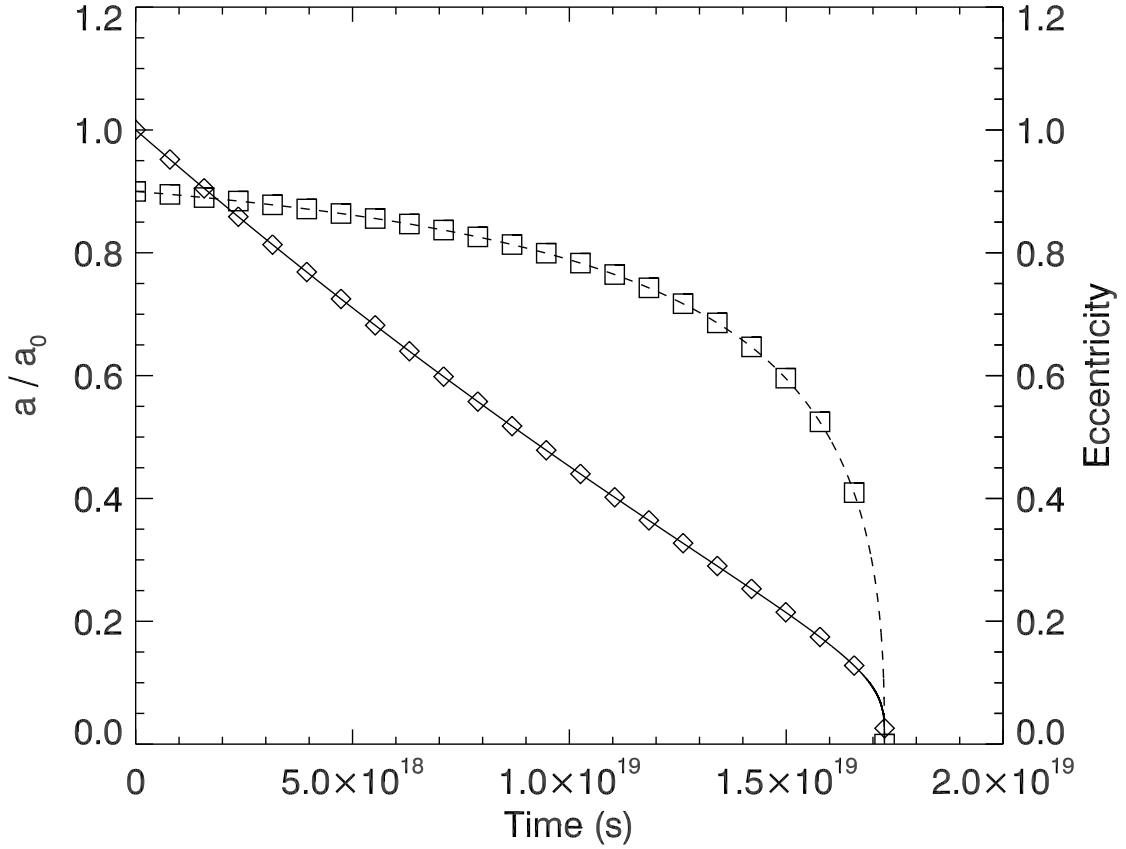


Fig. 1.— Comparison of HNDrag integration with numerical integration of Peters (1964) equations for an eccentric binary. Lines are numerical integration of Eq. 6 for semimajor axis (solid line) and of Eq. 7 for eccentricity (dashed line). The symbols are results from HNDrag integration with gravitational radiation for semimajor axis (diamonds) and eccentricity (squares). The binary shown has $m_0 = m_1 = 10 M_\odot$ with an initial orbit of $a_0 = 1$ AU and $e_0 = 0.9$. The evolution of the binary’s orbital elements is in very close agreement for the entire life of the binary.

where v_∞ is the relative velocity at infinity of the two masses. In Figure 2 we plot the orbits integrated both with and without gravitational radiation for two different sets of initial conditions that straddle the $r_{p,\max}$ threshold. For both sets of initial conditions, the integrations with gravitational radiation differ from the Newtonian orbits, and the inner orbit loses enough energy to become bound and ultimately merge. We used a bisection method of multiple integrations to calculate $r_{p,\max}$, and our value agrees with that of Quinlan & Shapiro (1989) to a fractional accuracy of better than 10^{-5} .

For systems of three or more masses, we compute gravitational radiation forces for each pair of objects and add them linearly. Although this method differs from the full relativistic treatment, which is nonlinear, the force from the closest pair almost always dominates. We may estimate the probability of a third object coming within the same distance by examining the timescales for an example system. A binary black hole system with $m_0 = 1000 M_\odot$ and $m_1 = 10 M_\odot$ with a separation $a = 10^{-2}$ AU ($\sim 1000M$) will merge within (Peters 1964)

$$\tau_{\text{merge}} \approx 6 \times 10^{17} \frac{(1 M_\odot)^3}{m_0 m_1 (m_0 + m_1)} \left(\frac{a}{1 \text{ AU}} \right)^4 (1 - e^2)^{7/2} \text{ yr} \approx 600 \text{ yr.} \quad (9)$$

The expression for merger time in Equation 9 is valid for the high eccentricities ($e \rightarrow 1$) of interest to this paper. The rate of gravitationally focused encounters with a third mass m_2 within a distance r from an isotropic distribution is (Paper I)

$$v_{\text{enc}} = 5 \times 10^{-8} \left(\frac{10 \text{ km s}^{-1}}{v_\infty} \right) \left(\frac{n}{10^6 \text{ pc}^{-3}} \right) \left(\frac{r}{1 \text{ AU}} \right) \left(\frac{m_0 + m_1}{1 M_\odot} \right) \left(\frac{m_2}{1 M_\odot} \right)^{1/2} \text{ yr}^{-1}. \quad (10)$$

For a number density $n = 10^6 \text{ pc}^{-3}$, a relative velocity $v_\infty = 10 \text{ km s}^{-1}$, and an interloper mass $m_2 = 10 M_\odot$, the rate of encounters within the same distance $r = a = 10^{-2}$ AU is $v_{\text{enc}} \sim 2 \times 10^{-6} \text{ yr}^{-1}$. Thus the probability of an encounter within the same distance is $P \sim \tau_{\text{merge}} v_{\text{enc}} \approx 10^{-3}$ for this mildly relativistic case. For a separation of 10^{-3} AU, the probability drops to 10^{-8} . Thus for most astrophysical scenarios and for all simulations in this paper, the error incurred from adding the gravitational radiation force terms linearly is negligible.

3. Simulations and Results

3.1. Individual Binary-Single Encounters

3.1.1. Close Approach

We begin our study of three-body encounters including gravitational radiation by calculating the minimum distance between any two objects during the binary-single scattering event. This

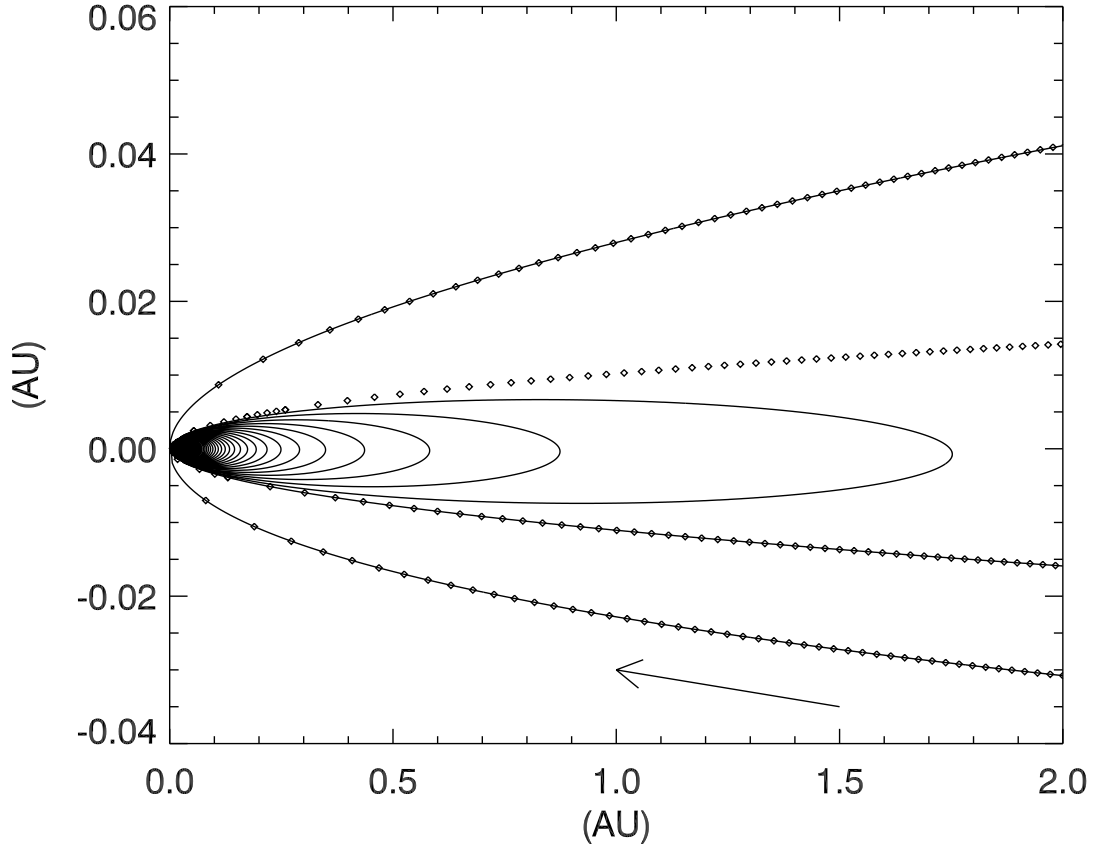


Fig. 2.— HNDrag-integrated orbits with and without gravitational radiation inside and outside of two-body capture pericenter. This plot shows orbits of two $10 M_{\odot}$ black holes with relative velocity of 10 km s^{-1} and pericenter distances of $r_p = 0.2r_{p,\text{max}}$ and $r_p = 1.2r_{p,\text{max}}$. The lines show the orbits with gravitational radiation included in the integration, and the diamonds show the Newtonian orbits for the same initial conditions. The direction of the orbit is indicated by the arrow. Although it is not apparent for the outer orbit in this plot, both trajectories differ from their Newtonian counterparts. For the inner orbit, enough energy is radiated away for the black holes to become bound to each other and eventually merge.

quantity has been well studied for the Newtonian case, but it is still not completely understood (Hut & Inagaki 1985; Sigurdsson & Phinney 1993). We present 10^5 simulations of a circular binary with masses $m_0 = m_1 = 1 M_\odot$ and an initial semimajor axis $a_0 = 1$ AU interacting with an interloper of mass $m_2 = 1 M_\odot$ in a hyperbolic orbit with respect to the center of mass of the binary. Throughout this paper, we refer to the mass ratios of three-body encounters as $m_0:m_1:m_2$, where m_2 is the interloper and the binary consists of m_0 and m_1 with $m_{\text{bin}} = m_0 + m_1$ and $m_0 \geq m_1$. The relative velocity of the binary and the interloper at infinity is $v_\infty = 0.5$ km s $^{-1}$ with an impact parameter randomly drawn from a distribution with a probability $P(b) \propto b$ and a maximum value $b_{\text{max}} = 6.621$ AU, which corresponds to a two-body pericenter distance of $r_p = 5a$. The encounters are integrated until finished as determined in Paper I while tracking the minimum distances between all pairs of objects. We follow Hut & Inagaki (1985) and Sigurdsson & Phinney (1993) in calculating a cumulative, normalized cross section for close approach less than r

$$\sigma(r) = \frac{f(r) b_{\text{max}}^2}{a_0^2} \left(\frac{v_\infty}{v_c} \right)^2, \quad (11)$$

where

$$v_c \equiv \sqrt{G \frac{m_0 m_1}{a m_2} \frac{(m_0 + m_1 + m_2)}{(m_0 + m_1)}} \quad (12)$$

is the minimum relative velocity required to ionize the system and $f(r)$ is the fraction of encounters that contain a close approach less than r . We plot $\sigma(r/a_0)$ for the Newtonian case at several different time intervals within the encounter in Figure 3. Our results for the total cross section are in almost exact agreement with Sigurdsson & Phinney (1993) over the domain of overlap, but with the advantage of ten years of computing advances, we were able to probe down to values of r/a_0 that are 10^2 times smaller. In addition we examine how the total cross section evolves from the initial close approach of the binary until the end of the interaction through subsequent near passes during long-lived resonant encounters. At the time of the interloper’s initial close approach with the binary, the cross section is dominated by gravitational focusing, and thus the first two curves in Figure 3 are well fit by power laws with slope of 1. As the interactions continue, resonant encounters with multiple close approaches are possible, and the cross section for small values of r/a_0 increases. Each successive, intermediate curve approaches the final cross section by a smaller amount because there are fewer encounters that last into the next time bin. A fit of two contiguous power laws to the final curve yields a break at $r/a_0 = 0.0102$ with slopes of 0.85 and 0.35 for the lower and upper portions, respectively. These values are very close to those obtained by earlier studies (Hut & Inagaki 1985; Sigurdsson & Phinney 1993). There is, however, no reason for a preferred scale for a Newtonian system, and simple models that assume close approaches are dominated by pericenter passage after an eccentricity kick cannot explain the lower slope. We numerically calculate $d(\log \sigma)/d(\log r)$ by fitting multiple lines to $\sigma(r)$ in logarithmic space and plot the results in Figure 4. The derivative $d(\log \sigma)/d(\log r)$ appears to approach unity for very

small values of r/a_0 where the close approach can be thought of as a gravitationally focused two-body encounter within the entire system (Hut & Inagaki 1985). It is surprising that this does not happen until $r/a_0 < 10^{-5}$.

In order to test the effects of gravitational radiation on the close approach as well as to test the sensitivity of the results to the phase of the binary, we ran the same simulations (1) with gravitational radiation, (2) with gravitational radiation and first-order post-Newtonian corrections, and (3) with just first-order post-Newtonian corrections. The three new cross sections are plotted with the Newtonian results in Figure 5. A K-S test shows the differences between the three curves to be statistically insignificant ($P \geq 0.4$). Although not statistically significant, the curves with gravitational radiation appear to drop below the Newtonian curve for small r/a_0 and then climb above for very small r/a_0 . Gravitational radiation causes this effect by driving objects that become very close to each other closer still and, in some cases, causing them to merge. For larger masses, the gravitational radiation is stronger, and the gravitational radiation curve will differ from the Newtonian curve at larger r/a_0 for a fixed value of a_0 .

3.1.2. Merger Cross Section

The most interesting new consequence from adding the effects of gravitational radiation to the three-body problem is the possibility of a merger between two objects. Though the two-body cross section for merger can be calculated from Equation 8, the dynamics of three-body systems increases this cross section in a nontrivial manner. We present simulations of individual binary-single encounters for a variety of masses. As in Paper I, the interactions were set up in hyperbolic encounters with a relative velocity at infinity of $v_\infty = 10 \text{ km s}^{-1}$ with an impact parameter distribution such that $P(b) \propto b$ with $b_{\min} = 0$ and b_{\max} such that the maximum pericenter separation would be $r_p = 5a$. The binaries were initially circular with semimajor axes ranging from 10^{-6} AU to 10^2 AU, depending on the mass. The masses were picked such that one of the three mass ratios was unity with all masses ranging from $10 M_\odot$ to $10^3 M_\odot$ with roughly half-logarithmic steps. For each mass and semimajor axis combination, we run 10^4 encounters. We calculate the merger cross section as $\sigma_m = f\pi b_{\max}^2$ where f is the fraction of encounters that resulted in a merger while all three objects were interacting. In Figures 6-9 we plot, as a function of the semimajor axis scaled to the gravitational radius of the binary $\xi \equiv a/(Gm_{\text{bin}}/c^2)$, the cross section normalized to the physical cross section of the Schwarzschild radius of the mass of the entire system taking gravitational focusing into account:

$$\bar{\sigma}_m = \sigma_m \left[4\pi \frac{GM_{\text{tot}}}{v_\infty^2} \frac{GM_{\text{tot}}}{c^2} \right]^{-1}. \quad (13)$$

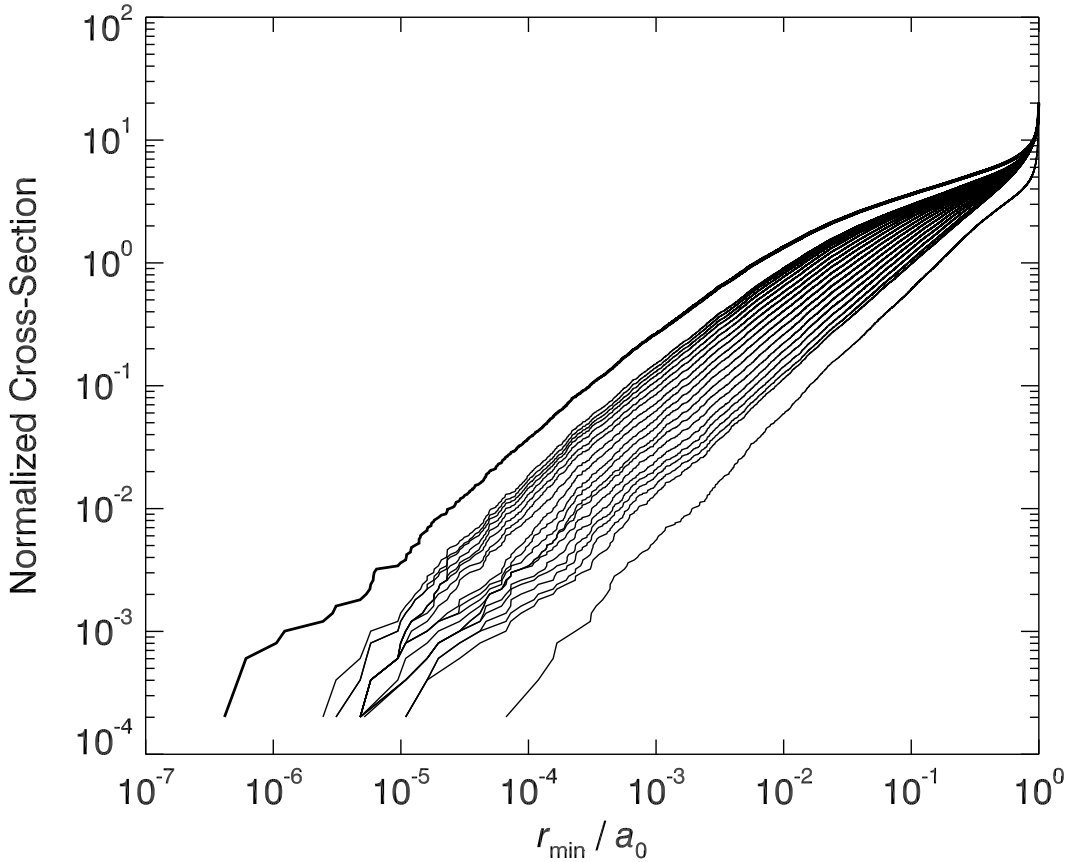


Fig. 3.— Cross section for close approach during binary-single encounters as a function of r_{\min}/a_0 . The thick, upper curve is the cross section for the entire encounter. The remaining curves are the cross section at intermediate, equally-spaced times during the encounter starting from the bottom near the time of initial close approach. Because we only include 20 intermediate curves, there is a gap between the last intermediate curve and the final curve. The first two curves have a slope of 1, consistent with close approach dominated by gravitational focusing. As the encounters progress, resonant encounters with multiple passes are more likely to have a close approach at smaller r_{\min}/a_0 , and the curves gradually evolve to the total cross section for the entire encounter.

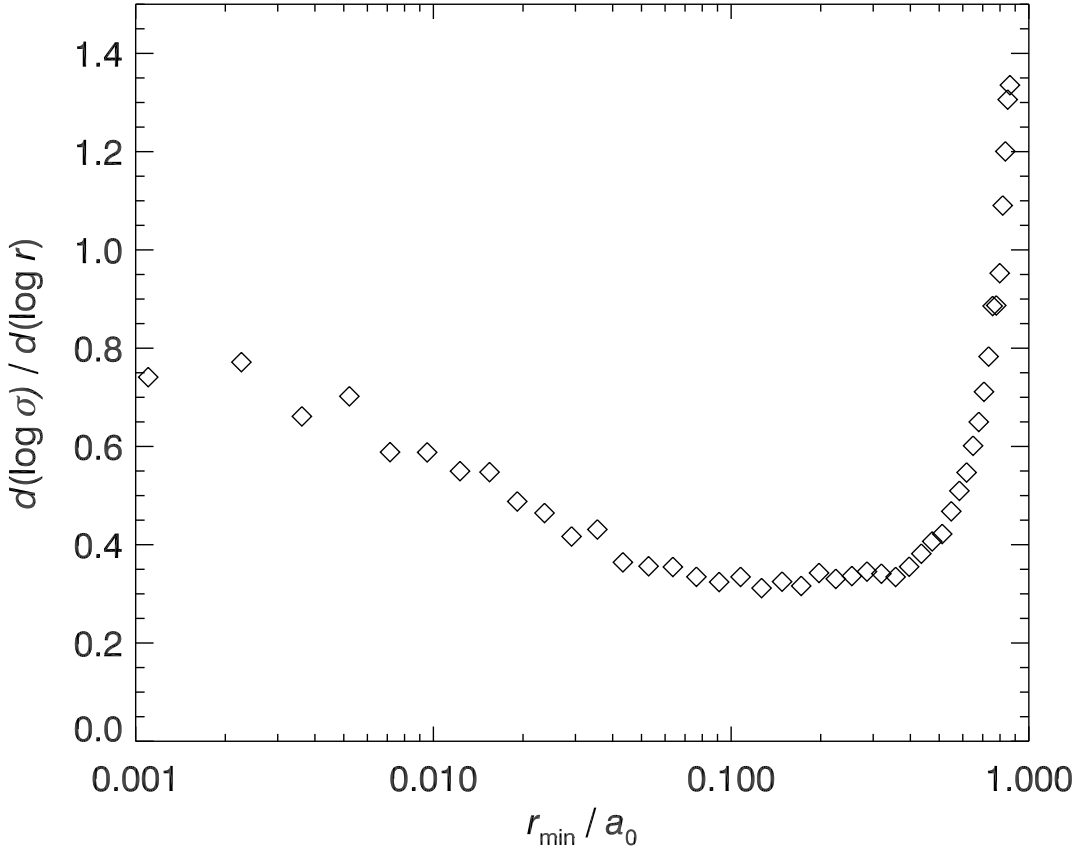


Fig. 4.— Derivative of close approach cross section curve for the entire encounter. Each symbol is the slope for a line segment fit to the top curve from Fig. 3 plotted as a function of the midpoint of the range. Because of the small number of encounters that result in very small close approaches, the multiple line segments used in the fits cover different ranges in $\log(r/a_0)$. They were selected so that each of the 100 line segments covers an additional 1000 encounters that make up the cumulative cross section curve. The scatter in the points is indicative of the statistical uncertainty. For smaller close approaches, $d(\log \sigma) / d(\log r)$ appears to approach unity. The rise at the right occurs because the cross section is formally infinite at $r_{\min}/a_0 = 1$.

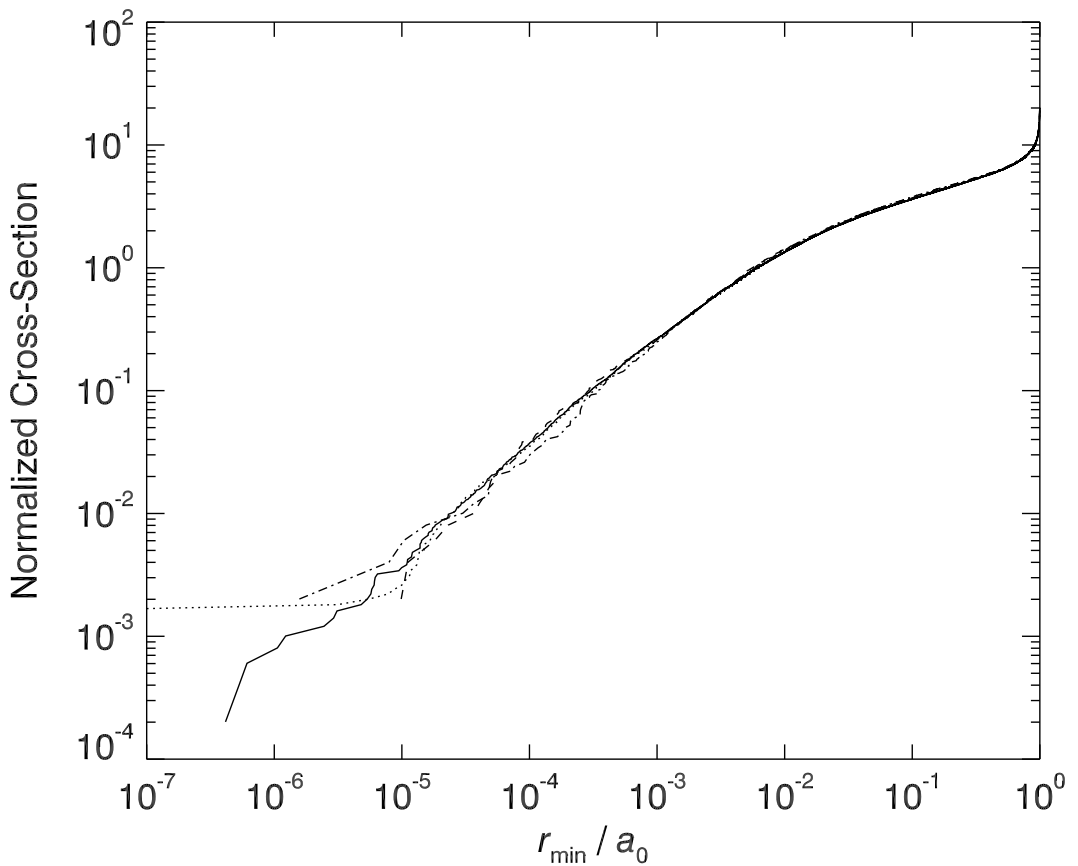


Fig. 5.— Cross section for close approach like Fig. 3 including different orders of Post-Newtonian corrections. The curves are purely Newtonian (solid), Newtonian plus 2.5-order PN (dotted), Newtonian plus 1-order PN (dashed), and Newtonian plus 1-order and 2.5-order PN (dash-dotted). The purely Newtonian and the Newtonian plus 2.5-order PN curves come from 10^5 encounters each. The other two curves come from 10^4 encounters each and show more statistical fluctuations. The differences between the curves are not statistically significant.

For all mass ratios $\bar{\sigma}_m$ increases with ξ because hard binaries with wide separations sweep out larger targets where the interloper can interact with and merge with the binary components. As ξ increases to the point that the binary is no longer hard, $\bar{\sigma}_m$ will approach the value expected from Equation 8. The curves flatten out for $\xi \lesssim 100$ as the cross section is dominated by the mergers of binary members with each other because of hardening interactions and eccentricity kicks that bring the two masses together. For sufficiently small ξ , the merger cross section would be formally infinite since all binaries would merge quickly. For all mass series, as the mass ratios approach unity, the cross section increases because complicated resonant encounters, which produce more numerous and smaller close approaches, are more likely when all three objects are equally important dynamically.

We note some interesting trends that can be seen in the plots. Note that for the scalings given, it is only the mass ratios that matter and not the absolute mass so that the 10:10:10 and 1000:1000:1000 cases only differ because of statistical fluctuations (Figs. 6 and 7). Thus our results can be scaled to others, e.g., 1000:100:100 would be the same as 100:10:10. For the 10:10:X mass series (Fig. 6), the normalized cross section decreases with increasing interloper mass, roughly as $\bar{\sigma}_m \sim (m_2/m_{\text{bin}})^{-1}$. This happens because as the interloper dominates the total mass of the system, complicated resonant interactions with more chances for close approach are less likely. Thus for the 10:10:1000 case, there are far fewer chances for a close approach that results in merger. The 1000:1000:X series (Fig. 7) shows a distinct break around $\xi \sim 100$. Since the binary mass is the same for all curves, they all approach the same value for $\xi \lesssim 100$ where the binary members merge with each other because of their small separation. For $\xi \gtrsim 100$, the higher mass interlopers are dynamically more important and cause more mergers. The X:10:10 series curves (Fig. 8) all approach the 10:10:10 curve for $\xi \gtrsim 10^5$ where the dominant object in the binary has less influence over its companion.

3.2. Sequences of Encounters

Because a tight binary in a dense stellar environment will suffer repeated encounters until it merges from gravitational radiation, we simulate a binary undergoing repeated interactions through sequences of encounters including gravitational radiation reaction. As in Paper I, we start with a circular binary with initial semimajor axis $a_0 = 10$ AU and a primary of mass $m_0 = 10, 20, 30, 50, 100, 200, 300, 500$, or $1000 M_{\odot}$ and a secondary of mass $m_1 = 10 M_{\odot}$. We simulate encounters with interloping black holes with mass $m_2 = 10 M_{\odot}$. After each encounter, we integrate Equations 6 and 7 to get the initial semimajor axis and eccentricity for the next encounter. This procedure continues until the binary merges from gravitational radiation or there is a merger during the encounter. Throughout our simulations we use an encounter velocity of $v_{\infty} = 10 \text{ km s}^{-1}$, an

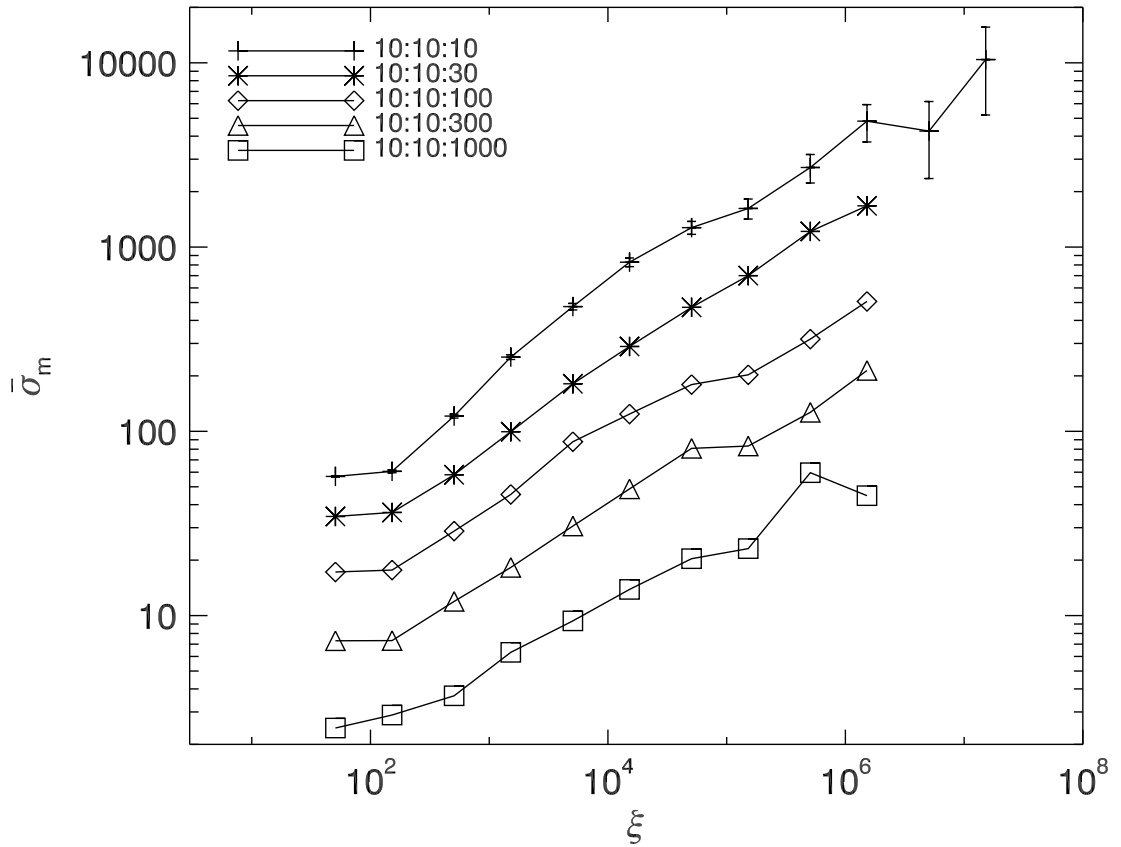


Fig. 6.— Normalized merger cross sections (Eq. 13) for individual binary-single encounters as a function of ξ for the 10:10:X mass series. The normalization is explained in the text. Each symbol represents 10^4 binary-single encounters. Error bars given for the top curve are representative for all merger cross section curves in Figures 6 through 9.

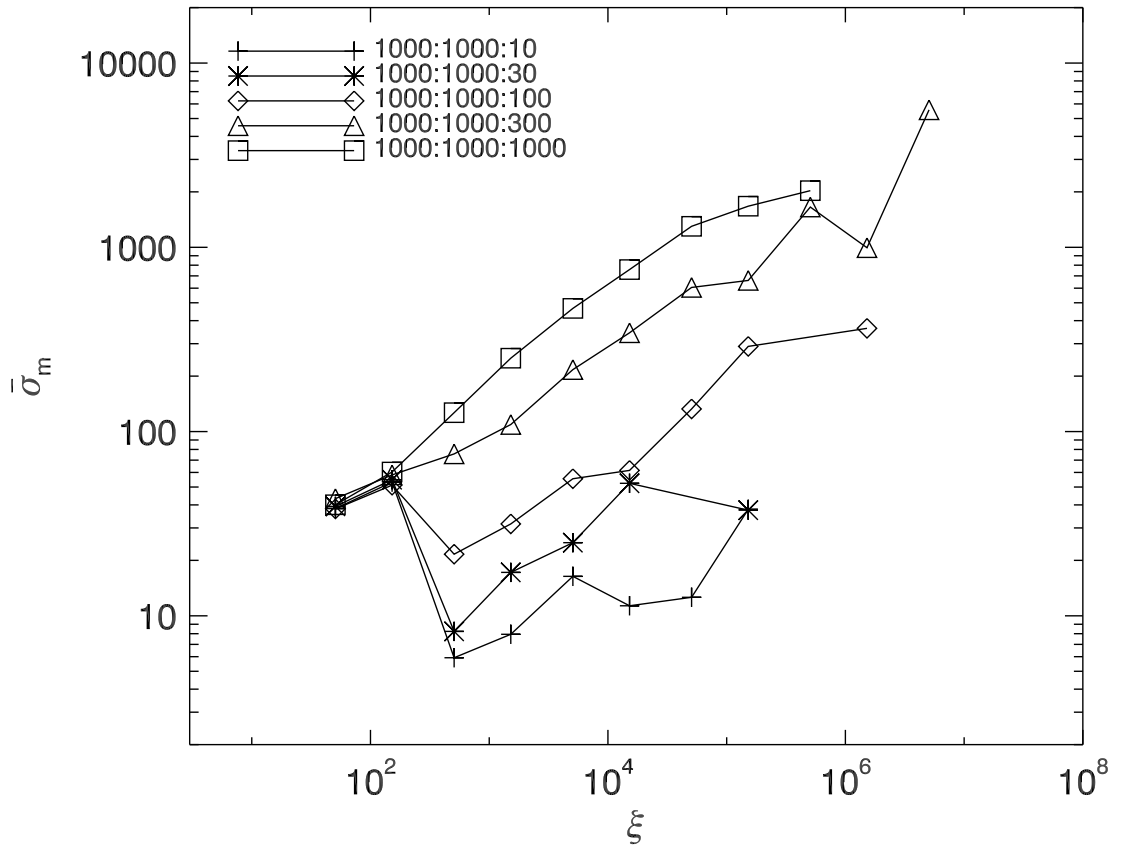


Fig. 7.— Normalized merger cross sections like Fig. 6 for 1000:1000:X series. The error bars from Figure 6 are representative for the curves in this figure.

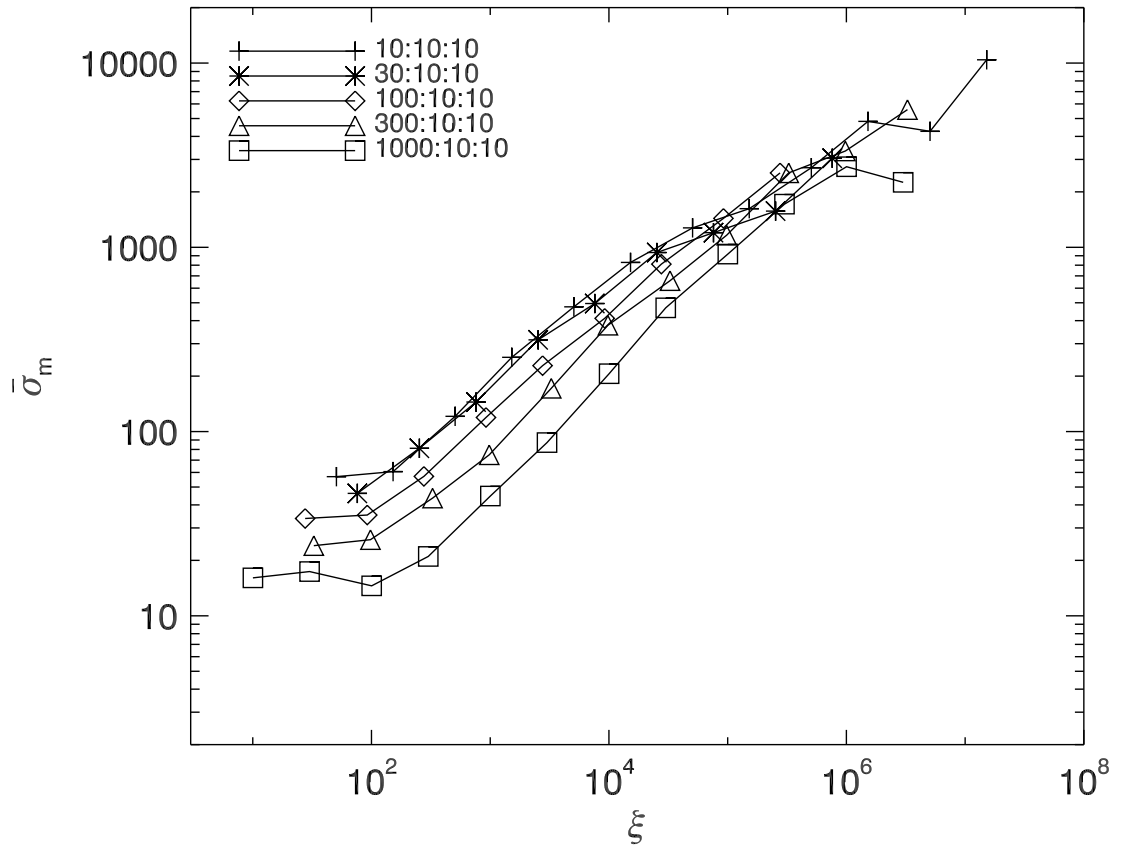


Fig. 8.— Normalized merger cross section like Fig. 6 for X:10:10 series. The error bars from Figure 6 are representative for the curves in this figure.

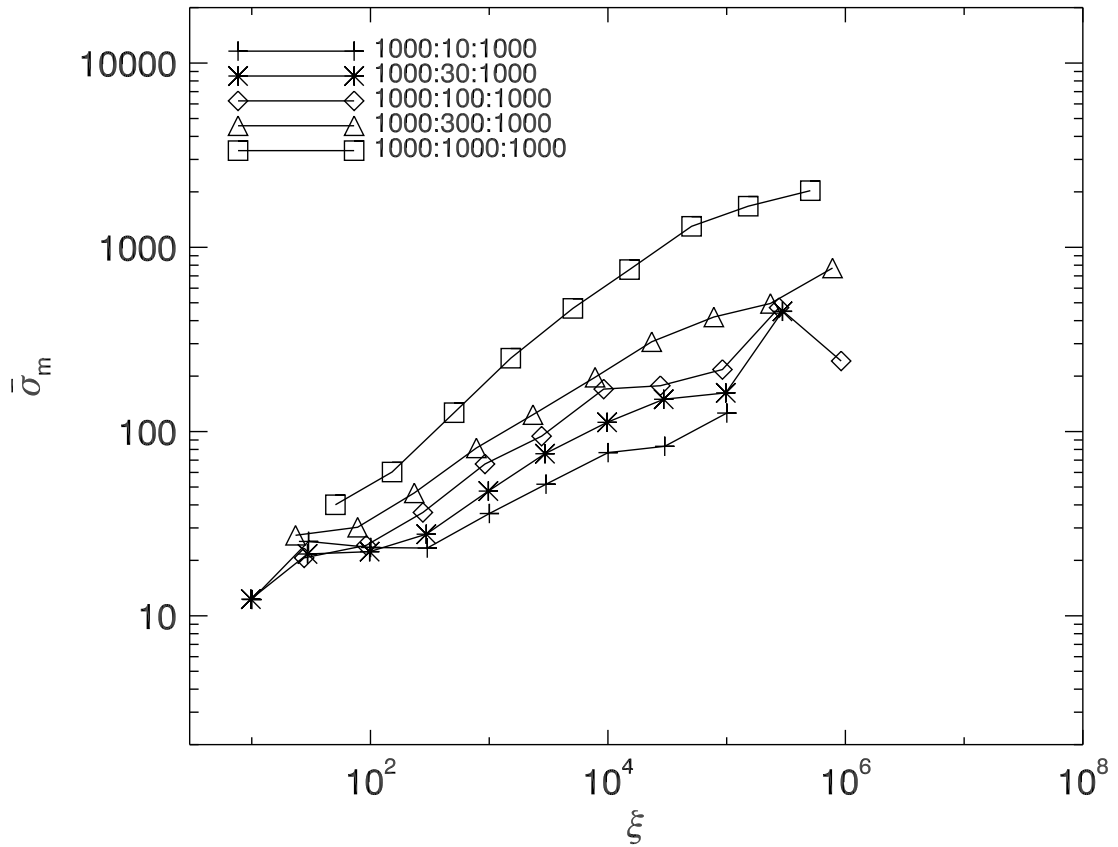


Fig. 9.— Normalized merger cross section like Fig. 6 for 1000:X:1000 series. The error bars from Figure 6 are representative for the curves in this figure.

isotropic impact parameter such that the hyperbolic pericenter would range from $r_p = 0$ to $5a$, and a black hole number density in the core $n = 10^5 \text{ pc}^{-3}$ (See Paper I for an explanation of these choices.). For each mass ratio we simulate 1000 sequences of encounters with gravitational radiation reaction.

Our results are summarized in Table 1. The inclusion of gravitational waves during the encounter makes a significant difference from the results reported in Paper I. The fraction of sequences that result in a merger during an encounter f_m is a good indicator of the importance of gravitational waves. Even for $m_0 = 10 M_\odot$, a significant fraction ($f_m > 0.1$) of the sequences merge this way, and for $m_0 > 300 M_\odot$ this type of merger is more likely to occur than mergers between encounters, and thus this effect shortens the sequence significantly. In particular, for $m_0 = 1000 M_\odot$ compared to the values from Paper I, the average number of encounters per sequence $\langle n_{\text{enc}} \rangle$ is decreased by 42%; the average number of black holes ejected from the cluster $\langle n_{\text{ej}} \rangle$ is reduced by 56%; and the average sequence length $\langle t_{\text{seq}} \rangle$ is 67% shorter. One caveat for the study of sequences of encounters is that an IMBH in a cluster of much lower mass objects will gather a large number of companions in elongated orbits through binary disruptions, and thus the picture of an isolated binary encountering individual black holes may not hold when the IMBH becomes very massive (Pfahl 2005).

4. Discussion

4.1. Implications for IMBH Formation and Growth

Our simulations provide a useful look into the merger history of an IMBH or its progenitor in a dense stellar cluster. As an IMBH grows through mergers with stellar-mass black holes, it will progress through the different masses that we included in our simulations of sequences. We interpolate the results in Table 1 to calculate the time it takes to reach $1000 M_\odot$, the number of cluster black holes ejected while building up to $1000 M_\odot$, and the probability of retaining the IMBH progenitor in the cluster for different seed masses and escape velocities of the cluster.

The time to build up to $1000 M_\odot$ is dominated by $\langle t_{\text{seq}} \rangle$ at high masses. Although each individual sequence is short, far more mergers are required for the same fractional growth in mass. In Figure 10 we plot the mass of the IMBH as a function of time for an initial mass of $m_0 = 10$, 50 , and $200 M_\odot$, for which total times to reach $1000 M_\odot$ are 600 , 400 , and 250 Myr, respectively. Because we assume a constant core density throughout the simulations, the times are unaffected by changing the cluster’s escape velocity. Without gravitational radiation, the times are roughly twice as long (Paper I) because the length of each sequence is dominated by the time it spends between encounters at small a when encounters are rarer. With gravitational radiation included,

Table 1. Sequence Statistics

m_0/M_\odot	$\langle n_{\text{enc}} \rangle$	$\langle n_{\text{ej}} \rangle$	f_{binej}	$\langle t_{\text{seq}} \rangle / 10^6 \text{ yr}$	$\langle a_f \rangle / \text{AU}$	$\langle e_f \rangle$	f_m
10	46.4	3.2	0.652	54.10	0.174	0.904	0.134
20	46.7	5.1	0.515	40.86	0.224	0.900	0.130
30	52.4	7.3	0.457	29.47	0.290	0.898	0.156
50	62.3	10.8	0.329	19.17	0.291	0.897	0.190
100	83.9	16.6	0.103	11.65	0.401	0.893	0.275
200	123.0	24.3	0.011	7.26	0.411	0.885	0.387
300	147.8	26.9	0.002	4.74	0.543	0.881	0.492
500	197.5	33.1	-	3.03	0.611	0.879	0.627
1000	284.2	38.8	-	1.47	0.878	0.914	0.754

Note. — Main results of simulations of sequences of encounters with gravitational radiation included during the encounter. The columns are: the mass of the dominant black hole m_0 , the average number of encounters per sequence $\langle n_{\text{enc}} \rangle$, the average number per sequence of stellar-mass black holes ejected from a stellar cluster with escape velocity 50 km s^{-1} $\langle n_{\text{ej}} \rangle$, the fraction of sequences in which the binary is ejected f_{binej} from a stellar cluster with escape velocity 50 km s^{-1} , the average time per sequence $\langle t_{\text{seq}} \rangle$, the average final semimajor axis of the binaries after the last encounter $\langle a_f \rangle$, the average final eccentricity of the binaries after the last encounter $\langle e_f \rangle$, and the fraction of sequences that end with a merger during the encounter f_m . Note that $\langle a_f \rangle$ and $\langle e_f \rangle$ only refer to the binaries that do not merge during the encounter; these comprise $1 - f_m$ of the sequences.

mergers that occur during an encounter are more likely at small separations, and the length of the sequence is shortened. These times are much shorter than the age of the globular cluster and are smaller than or comparable to timescales for ejection of black holes from the cluster, which we discuss below (see also Portegies Zwart & McMillan 2000; O’Leary et al. 2005). Thus time is not a limiting factor in reaching $1000 M_{\odot}$ for an IMBH progenitor that can remain in a dense cluster with a sufficiently large population of stellar mass black holes.

Each time that an encounter tightens the binary, energy is transferred to the interloper, which leaves with a higher velocity. If energetic enough, this interaction will kick the interloper out of the cluster. If the interactions kick all of the interacting black holes out of the cluster, the IMBH cannot continue to grow. In a dense cluster, there are roughly 10^3 black holes (Paper I). With gravitational radiation included during the encounters, the number of black holes ejected is roughly halved (Fig. 11), but the total number ejected while building up to $1000 M_{\odot}$ is still a few times the number of black holes available even for an escape velocity of $v_{\text{esc}} = 70 \text{ km s}^{-1}$. Thus a black hole smaller than $m_0 \lesssim 600 M_{\odot}$ cannot reach $1000 M_{\odot}$ by this method without additional processes such as Kozai resonances (Gültekin et al. 2004; Miller & Hamilton 2002a; Wen 2003, though O’Leary et al. 2005 find that Kozai-resonance induced mergers will only increase the total number of mergers by $\sim 10\%$). There is still the potential for significant growth in a short period of time. If we consider the point at which half of the black holes have been ejected from the cluster as the end of growth, then a black hole with initial mass of $50 M_{\odot}$ will grow to $290 M_{\odot}$ in 120 Myr, and a black hole of $200 M_{\odot}$ will grow to $390 M_{\odot}$ in less than 100 Myr. In addition, this ejection of stellar-mass black holes by a binary with a large black hole is faster than by self-ejection from interactions among stellar-mass black holes calculated by Portegies Zwart & McMillan (2000), who find that $\sim 90\%$ of black holes are ejected in a few Gyr. O’Leary et al. (2005), however, find that the inclusion of a mass spectrum of black holes further speeds up the ejection of stellar-mass black holes.

For every kick imparted on an interloper, conservation of momentum ensures a kick on the binary. Even with a large black hole, extremely large kicks can eject the binary from the cluster, at which point the IMBH progenitor can no longer grow. We can calculate the probability of IMBH retention for an individual sequence as $1 - f_{\text{binej}}$, from which we interpolate the probability of remaining in the cluster while growing to $300 M_{\odot}$ when the binary is essentially guaranteed to remain in the cluster. We plot this probability as a function of seed mass for several different escape velocities in Figure 12. The inclusion of gravitational waves during the encounter increases the retention probability for small masses. For $m_0 = 50 M_{\odot}$ the cluster retains the binary more than 12% of the time, and 49% of the time for $m_0 = 100 M_{\odot}$. Because the energy that an interloper can carry away from the system scales as

$$\Delta E \sim \frac{m_1}{m_0 + m_1} |E_B| = \frac{m_1}{m_0 + m_1} \frac{Gm_0m_1}{2a}, \quad (14)$$

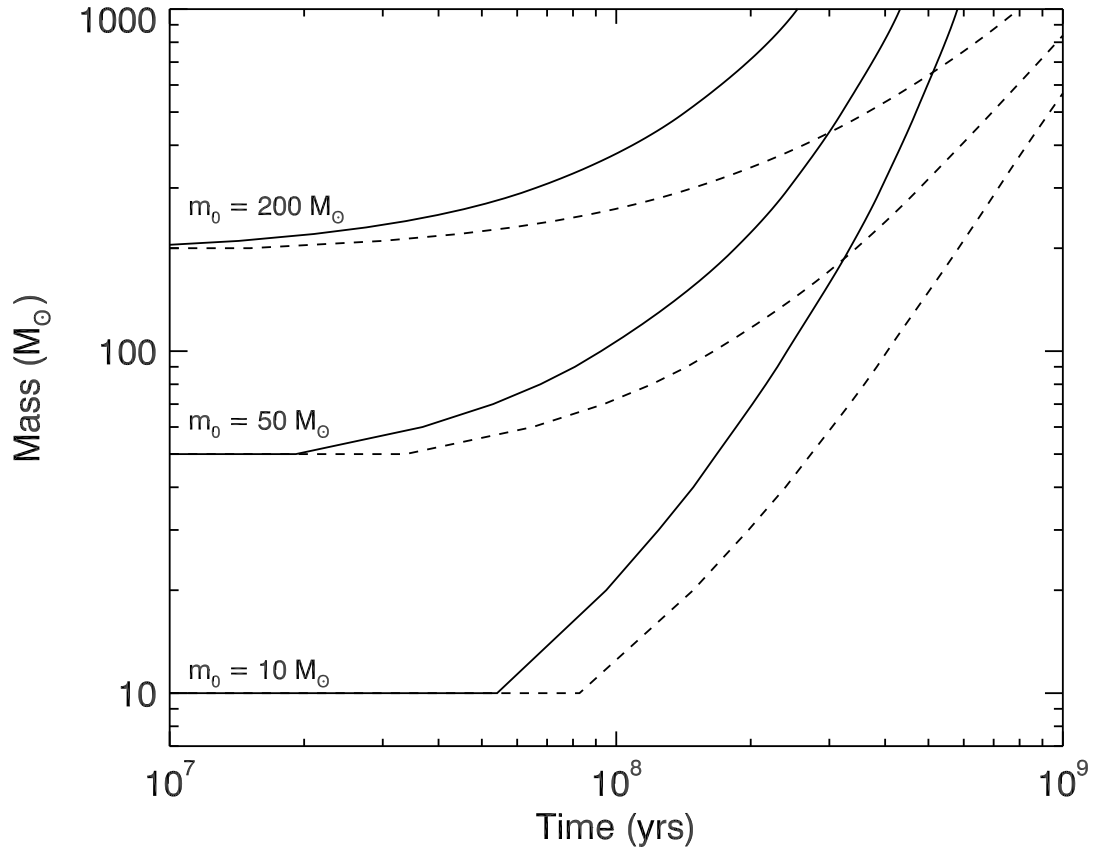


Fig. 10.— Mass of progenitor IMBH as a function of time as it grows through mergers with $10 M_\odot$ black holes in a dense stellar cluster. Solid curves show results from this work in which gravitational radiation is included, and dashed curves show results from Paper I in which this effect is ignored. From bottom to top the curves show the growth of black holes with initial mass $m_0 = 10$, 50 , and $200 M_\odot$. The IMBH progenitors all reach $1000 M_\odot$ in less than 600 Myr, and the inclusion of gravitational radiation significantly speeds up the growth of the black hole.

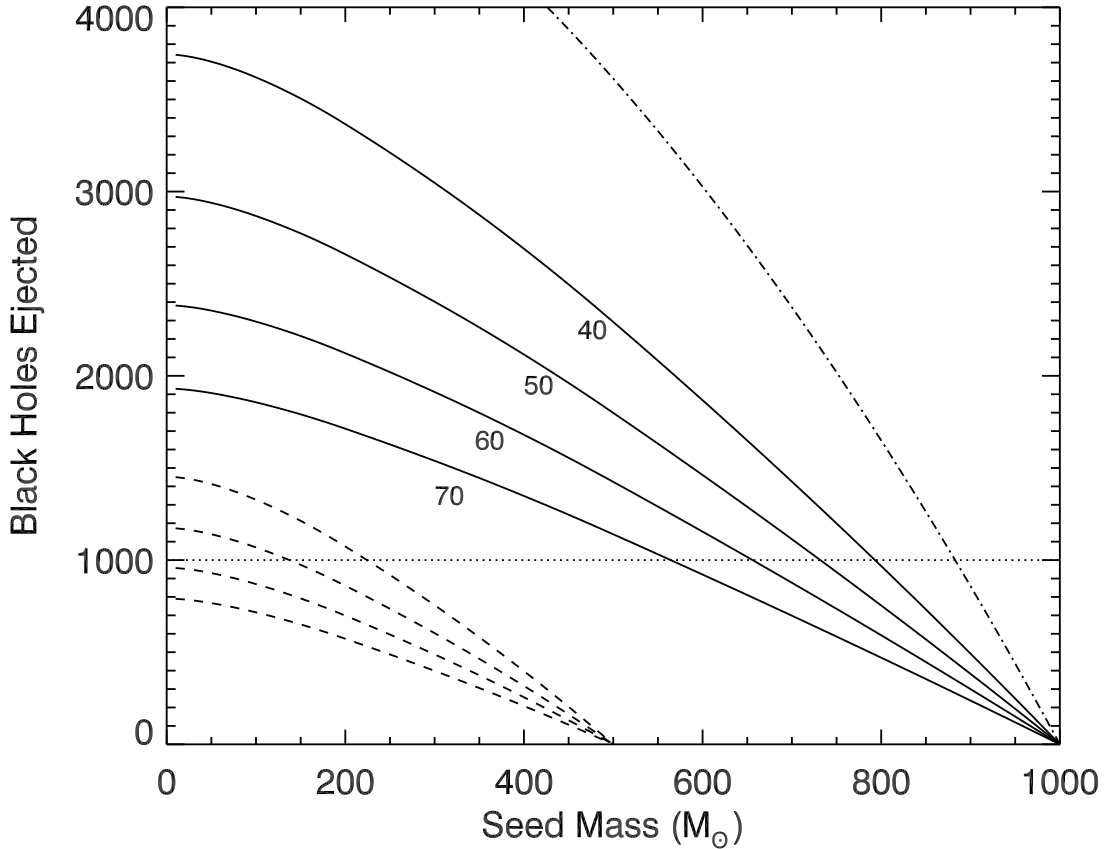


Fig. 11.— Number of black holes ejected in building up to $1000 M_{\odot}$ (solid curves) and to $500 M_{\odot}$ (dashed curves) as a function of seed mass for different cluster core escape velocities, given in units of km s^{-1} . The dotted line indicates the expected number of black holes in a dense globular cluster. The dot-dashed curve from Paper I shows the number of black holes ejected from the cluster in building up to $1000 M_{\odot}$ for a cluster escape velocity of 50 km s^{-1} without the effects of gravitational waves during the encounter. For all but the largest seed masses, the globular cluster does not contain enough black holes for the IMBH to reach $1000 M_{\odot}$. There are, however, a sufficient number of black holes to build up to $500 M_{\odot}$ for a seed mass greater than $225 M_{\odot}$ or an escape velocity of at least 60 km s^{-1} . The inclusion of gravitational radiation during the encounter roughly halves the number of ejections.

the encounters at the end of the sequence, when a is smallest, are the most likely to impart a kick large enough to eject the binary from the cluster. This is also the point at which effects from gravitational radiation are strongest and at which close encounters are most likely to cause a merger. When the encounter ends in a merger, there can be no more ejections. The mergers from gravitational radiation decrease the number of ejections by decreasing the number of encounters and thus the number of possible ejections as well as cutting off what would otherwise be the end of the sequence, in which ejections are more likely to occur.

Our analysis of the ejection of stellar-mass black holes as well as of IMBH progenitors does not include the effects of gravitational radiation recoil. As two objects with unequal masses or with misaligned spins spiral in towards each other, asymmetric emission of gravitational radiation produces a recoil velocity on the center of mass of the binary. Most of the recoil comes from contributions after the masses are inside of the ISCO, where post-Newtonian analysis becomes difficult (Favata et al. 2004). For non-spinning black holes, the velocity kick from the recoil up to the ISCO is (Favata et al. 2004)

$$v_r = 15.6 \text{ km s}^{-1} \frac{f(q)}{f_{\max}} \quad (15)$$

where $q = m_1/m_0 < 1$, $f(q) = q^2(1-q)/(1+q)^5$, and $f_{\max} \approx f(0.38) = .018$. Favata et al. (2004) bounded the total recoil to between $20 \text{ km s}^{-1} \leq v_r \leq 200 \text{ km s}^{-1}$ for non-spinning black holes with $q = 0.127$. Since the recoil velocity scales as q^2 for $q \ll 1$, this may be scaled to other mass ratios. More recently, Blanchet et al. (2005) argued from high order post-Newtonian expansions that the kick speed for very small mass ratios $q \ll 1$ was $v_r/c = 0.043q^2$, with an uncertainty of roughly 20%. This is consistent with the results of Favata et al. (2004), but as most of the recoil originates well inside the ISCO, Blanchet et al. (2005) caution that numerical results may be required for definitive answers. In both cases, a seed mass of $m_0 = 150 M_{\odot}$ merging with $m_1 = 10 M_{\odot}$ companions will produce a recoil velocity $v_r \lesssim 50 \text{ km s}^{-1}$. A seed mass greater than $150 M_{\odot}$ will then avoid ejection both from dynamical interactions and from gravitational radiation recoil.

4.2. Implications for Gravitational Wave Detection

In addition to the likelihoods and rates of growth of black holes in dense stellar systems, our simulations shed light on the gravitational wave signals that come from the mergers of these black holes. Making optimistic assumptions, O’Leary et al. (2005) calculate upper limits for Advanced LIGO detection rates of all black hole mergers in stellar clusters formed at a redshift $z = 7.8$. For their wide range of cluster properties, they find detection rates ranging from $v_{\text{LIGO}} \approx 0.6$ to 10 yr^{-1} . For cluster parameters that most closely resemble those used in Paper I and in this work

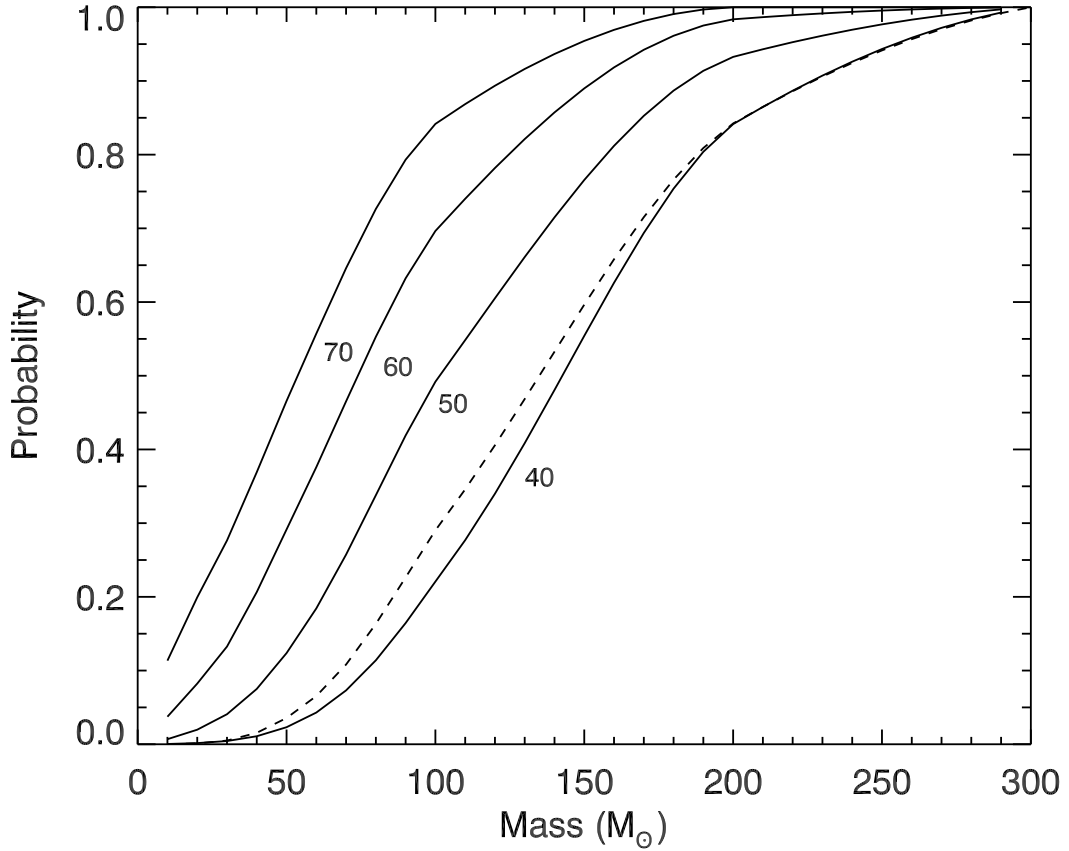


Fig. 12.— Probability for a binary with an IMBH to remain in the cluster until building up to $300 M_{\odot}$ as a function of seed mass for different cluster core escape velocities given in units of km s^{-1} . Solid curves are results from this work, and the dashed curve is from Paper I for an escape velocity of 50 km s^{-1} . The inclusion of gravitational radiation significantly increases the retention probability.

(GMH model series), they find $v_{\text{LIGO}} \approx 2$ to 4 yr^{-1} . Our simulations show that when gravitational radiation is included in the integration the number of black holes ejected per merger decreases for all mass ratios. With fewer black holes ejected from the cluster, the overall rate of black hole mergers increases. For the 10:10:10 case, the number of ejections per merger decreases by $\sim 10\%$, and for the 1000:10:10 case the number decreases by more than a factor of 2, thus increasing the rates found by O’Leary et al. (2005). The exact increase in rate is difficult to estimate because the total number of mergers is dominated by mergers between stellar-mass black holes yet the most easily detected mergers involve black holes with larger masses.

Because dynamical interactions strongly affect the eccentricity of a binary and because the timescale for merger is a such a strong function of eccentricity, binaries in a cluster tend to have very high eccentricities after their last encounter (Paper I, O’Leary et al. 2005). With the addition of gravitational radiation during the encounter, we find that the merging binaries become more eccentric because a significant fraction of the mergers (f_m in Table 1) occur during the encounter. These mergers typically happen between two black holes that are not bound to each other until they come close to each other and emit a significant amount of gravitational radiation, after which the two black holes are in an extremely high eccentricity orbit ($1 - e \lesssim 10^{-3}$).

To see how these high eccentricities affect the detectability of the gravitational wave signal, we integrate Equations 6 and 7 until the binaries are detectable by *LISA* and then Advanced LIGO. For circular orbits, the frequency of gravitational wave emission is twice the orbital frequency, but masses in eccentric orbits emit at all harmonics: $f_{\text{GW}} = n\Omega/2\pi$, where n is the harmonic number and

$$\Omega = \left[\frac{G(m_0 + m_1)}{a^3} \right]^{1/2} \quad (16)$$

with peak harmonic for $e > 0.5$ at approximately $n = 2.16(1 - e)^{-3/2}$ (Farmer & Phinney 2003). We consider the binary to be detectable by *LISA* when the peak harmonic frequency is between 2 mHz and 10 mHz. We plot the distribution of eccentricities in Figure 13. The distributions are essentially a combination of those from Figure 9 of Paper I and a sharp peak near $e = 1$, which comes from the mergers during the encounter. The number in the sharp peak increases with mass as f_m increases such that for 1000:10:10 more than 75% of the merging binaries detectable by LISA have an eccentricity greater than 0.9. Between 15% and 25% of all of the merging binaries have eccentricities so high that the peak harmonic frequency is above the most sensitive region of the LISA band, but they should still be emitting strongly enough at other harmonics to be detectable. Such high eccentricity presents challenges for the detection of these signals from the data of space-based gravitational wave detectors because (1) it requires a more computationally expensive template matching that includes non-circular binaries and (2) the binaries only emit a strong amount of gravitational radiation during the short time near periape as they merge. For a given semimajor axis, these extremely high eccentricities will also increase the gravitational wave

flux emitted and thus increase the distance out to which *LISA* can detect them, but the detection rate may be compensated by the fact that more parameters are required (Will 2004). We also integrate the orbital elements of the binaries until they are in the Advanced LIGO band ($40 \text{ Hz} < f_{\text{GW}} < f_{\text{ISCO}}$) or within a factor of 2 of their ISCO frequency for $m_0 > 100 M_{\odot}$. We find that they have almost completely circularized (Fig. 14). A tiny fraction ($< 0.5\%$) of the runs with $m_0 = 500$ and $1000 M_{\odot}$ have merging binaries with eccentricities such that $1 - e \lesssim 10^{-6}$.

5. Conclusions

1. *Gravitational radiation in N-body*. We present results of numerical simulations of binary-single scattering events including the effects of gravitational radiation during the encounter. We include gravitational radiation by adding the 2.5-order post-Newtonian force term (Eq. 5) to the equation of motion within the HNDrag framework. The code reproduces the expected semimajor axis and eccentricity evolution, and it gives the expected two-body capture radius.

2. *Close approach and merger cross sections*. We use the new code to test the effects of gravitational radiation on a standard numerical experiment of binary-single encounters. We probe the close approach cross section to smaller separations than has been simulated previously and find that the inclusion of gravitational radiation makes little difference except for extremely close encounters ($r_p < 10^{-5}a$), at which point gravitational radiation drives the objects closer together. We also present the cross section for merger during binary-single scattering events for a variety of mass ratios and semimajor axes.

3. *IMBH growth in dense stellar clusters*. We simulate sequences of binary-single black hole encounters to test for the effects of gravitational radiation and to test formation and growth models for intermediate-mass black holes in stellar clusters. We find that the inclusion of gravitational radiation speeds up the growth of black holes by a factor of 2, increases the retention of IMBH progenitors by a factor of 2, and decreases the ejection of stellar-mass black holes by a factor of 2. All of these effects act to enhance the prospects for IMBH growth.

4. *Detectability of gravitational waves*. We analyzed the merging binaries from the simulations of black holes in dense stellar clusters to look at the detectability of the gravitational wave signals from these sources. We find that the mergers that occur rapidly during the encounter as opposed to those that occur after the final encounter are an important source of black hole mergers, becoming the dominant source of mergers at the higher mass ratios. The mergers that do occur during the encounter tend to have extremely high eccentricity ($e > 0.9$) while in the *LISA* band, presenting challenges for their detection. When the gravitational wave signal from the merging black holes is in the Advanced LIGO band, the orbit will have completely circularized.

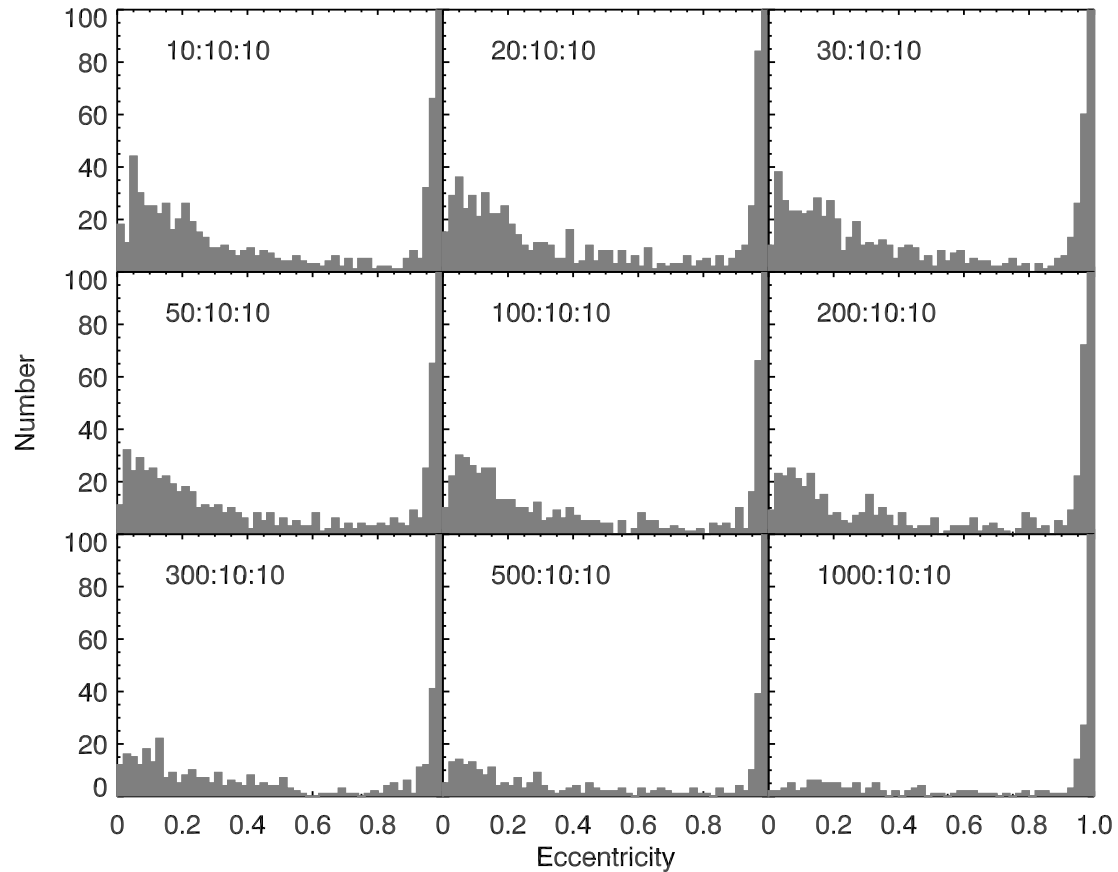


Fig. 13.— Histogram of eccentricities of merging binary while in the *LISA* band ($f_{GW} = 2$ mHz to 10 mHz) out of a total of 1000 sequences. The histograms show a combination of the binaries that merged after the last encounter with eccentricities concentrated around $0 < e \lesssim 0.3$ and the black holes that merged quickly during the encounter with eccentricities very close to unity. The peaks in the rightmost bin in all plots lie above the range of the plots.

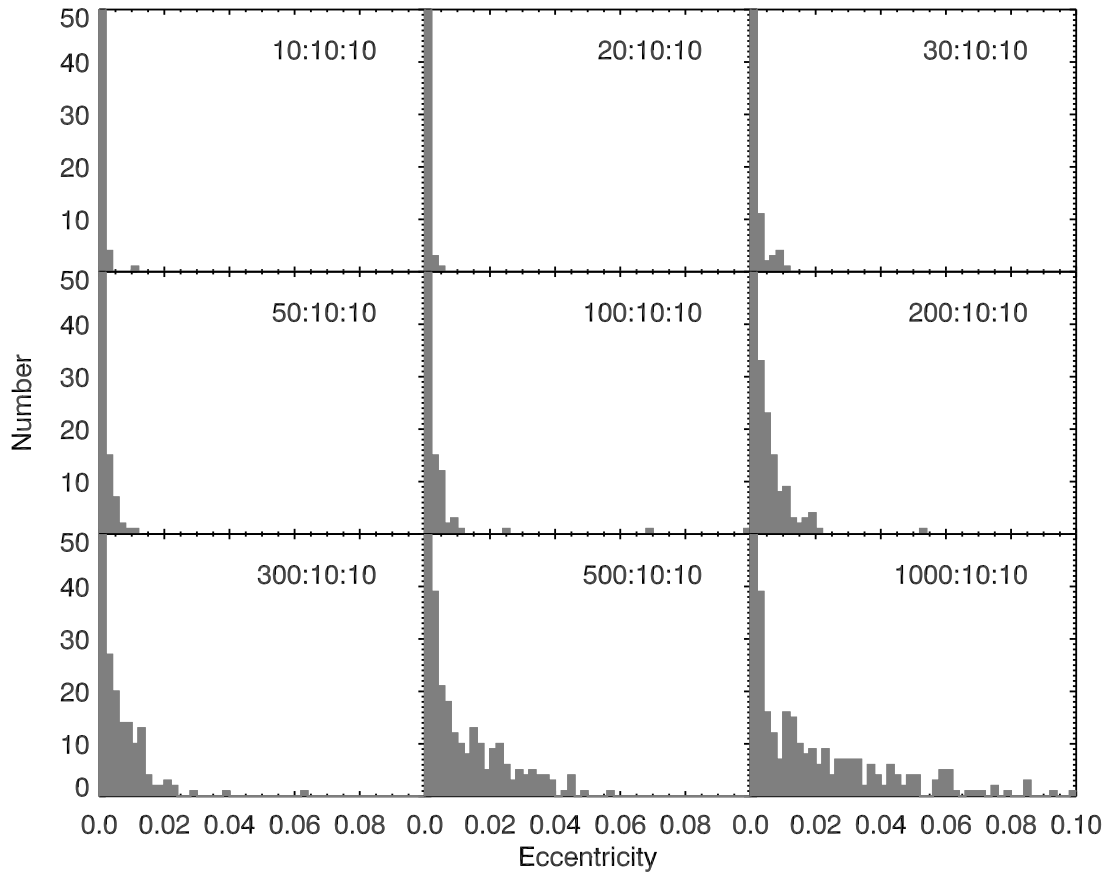


Fig. 14.— Histogram of eccentricities of merging binary while the gravitational wave frequency is detectable from current and future ground-based detectors. The upper limit of the frequency range is the ISCO frequency. We used a lower limit for frequency range of 100 Hz for $m_0 = 10$, and $20 M_\odot$; 35 Hz for $m_0 = 30, 50$, and $100 M_\odot$; and half the ISCO frequency for the higher mass binaries. The binaries are very close to circular once they are in the frequency range of ground-based detectors. The peaks in the rightmost bin in all plots lie above the range of the plots.

We are grateful for the hospitality of the Center for Gravitational Wave Physics and for suggestions from the anonymous referee. Many of the results in this paper were obtained using VAMPIRE, the Very Awesome Multiple Processor Integrated Research Environment, and the Beowulf cluster of the University of Maryland Department of Astronomy. This research has made use of NASA's Astrophysics Data System. This work was supported by NASA grant NAG 5-13229.

REFERENCES

Ando, M. & the TAMA collaboration. 2002, Classical and Quantum Gravity, 19, 1409

Angelini, L., Loewenstein, M., & Mushotzky, R. F. 2001, ApJ, 557, L35

Barish, B. C. 2000, Advances in Space Research, 25, 1165

Begelman, M. C. 2002, ApJ, 568, L97

Blanchet, L., Faye, G., & Ponsot, B. 1998, Phys. Rev. D, 58, 124002

Blanchet, L., Qusailah, M. S. S., & Will, C. M. 2005, [arXiv:astro-ph/0507692](https://arxiv.org/abs/astro-ph/0507692)

Colpi, M., Mapelli, M., & Possenti, A. 2003, ApJ, 599, 1260

Colpi, M., Possenti, A., & Gualandris, A. 2002, ApJ, 570, L85

Cutler, C. & Thorne, K. S. 2002, [arXiv:gr-qc/0204090](https://arxiv.org/abs/gr-qc/0204090)

Damour, T. 1982, C.R. Acad. Sc. Paris, Série II, 294, 1355

Damour, T. 1983, in Gravitational Radiation, edited by N. Deruelle and T. Piran, North-Holland, Amsterdam, 59–144

Damour, T. & Deruelle, N. 1981, Physics Letters A, 87, 81

Danzmann, K. 2000, Advances in Space Research, 25, 1129

Ebisuzaki, T., Makino, J., Tsuru, T. G., Funato, Y., Portegies Zwart, S., Hut, P., McMillan, S., Matsushita, S., Matsumoto, H., & Kawabe, R. 2001, ApJ, 562, L19

Fabbiano, G., Zezas, A., & Murray, S. S. 2001, ApJ, 554, 1035

Farmer, A. J. & Phinney, E. S. 2003, MNRAS, 346, 1197

Favata, M., Hughes, S. A., & Holz, D. E. 2004, ApJ, 607, L5

Ferraro, F. R., Possenti, A., Sabbi, E., Lagani, P., Rood, R. T., D’Amico, N., & Origlia, L. 2003, *ApJ*, 595, 179

Fidecaro, F. & VIRGO Collaboration. 1997, in General Relativity and Gravitational Physics; Proceedings of the 12th Italian Conference, edited by M. Bassan, V. Ferrari, M. Francaviglia, F. Fucito, and I. Modena. World Scientific Press, 1997., p.163, 163

Flanagan, É. É. & Hughes, S. A. 1998a, *Phys. Rev. D*, 57, 4535

—. 1998b, *Phys. Rev. D*, 57, 4566

Fryer, C. L. & Kalogera, V. 2001, *ApJ*, 554, 548

Gebhardt, K., Kormendy, J., Ho, L. C., Bender, R., Bower, G., Dressler, A., Faber, S. M., Filippenko, A. V., Green, R., Grillmair, C., Lauer, T. R., Magorrian, J., Pinkney, J., Richstone, D., & Tremaine, S. 2000, *ApJ*, 543, L5

Gebhardt, K., Rich, R. M., & Ho, L. C. 2002, *ApJ*, 578, L41

—. 2005, *ApJ*, 999, L999

Gerssen, J., van der Marel, R. P., Gebhardt, K., Guhathakurta, P., Peterson, R. C., & Pryor, C. 2002, *AJ*, 124, 3270

Gültekin, K., Miller, M. C., & Hamilton, D. P. 2004, *ApJ*, 616, 221

Gürkan, M. A., Freitag, M., & Rasio, F. A. 2004, *ApJ*, 604, 632

Hopman, C. & Portegies Zwart, S. 2005, [arXiv:astro-ph/0506181](https://arxiv.org/abs/astro-ph/0506181)

Hut, P. & Inagaki, S. 1985, *ApJ*, 298, 502

Itoh, Y., Futamase, T., & Asada, H. 2001, *Phys. Rev. D*, 63, 064038

Kaaret, P., Ward, M. J., & Zezas, A. 2004, *MNRAS*, 351, L83

King, A. R., Davies, M. B., Ward, M. J., Fabbiano, G., & Elvis, M. 2001, *ApJ*, 552, L109

Lee, M. H. 1993, *ApJ*, 418, 147

Martel, K. & Poisson, E. 1999, *Phys. Rev. D*, 60, 124008

Matsubayashi, T., Shinkai, H., & Ebisuzaki, T. 2004, *ApJ*, 614, 864

McCrady, N., Gilbert, A. M., & Graham, J. R. 2003, *ApJ*, 596, 240

Miller, J. M., Fabian, A. C., & Miller, M. C. 2004, *ApJ*, 614, L117

Miller, M. C. 2002, *ApJ*, 581, 438

Miller, M. C. & Colbert, E. J. M. 2004, *International Journal of Modern Physics D*, 13, 1

Miller, M. C. & Hamilton, D. P. 2002a, *ApJ*, 576, 894

—. 2002b, *MNRAS*, 330, 232

Newhall, X. X., Standish, E. M., & Williams, J. G. 1983, *A&A*, 125, 150

O’Leary, R. M., Rasio, F. A., Fregeau, J. M., Ivanova, N., & O’Shaughnessy, R. 2005, [arXiv:astro-ph/0508224](https://arxiv.org/abs/astro-ph/0508224)

Pakull, M. W. & Mirioni, L. 2001, in *Astronomische Gesellschaft Meeting Abstracts*, 112–+

Peters, P. C. 1964, *Physical Review*, 136, 1224

Pfahl, E. 2005, *ApJ*, 626, 849

Portegies Zwart, S. F., Baumgardt, H., Hut, P., Makino, J., & McMillan, S. L. W. 2004, *Nature*, 428, 724

Portegies Zwart, S. F. & McMillan, S. L. W. 2000, *ApJ*, 528, L17

—. 2002, *ApJ*, 576, 899

Quinlan, G. D. & Shapiro, S. L. 1989, *ApJ*, 343, 725

Ruszkowski, M. & Begelman, M. C. 2003, *ApJ*, 586, 384

Schilling, R. 1998, in *AIP Conf. Proc. 456: Laser Interferometer Space Antenna, Second International LISA Symposium on the Detection and Observation of Gravitational Waves in Space*, 217–221

Sigurdsson, S. & Phinney, E. S. 1993, *ApJ*, 415, 631

Strohmayer, T. E. & Mushotzky, R. F. 2003, *ApJ*, 586, L61

Wen, L. 2003, *ApJ*, 598, 419

Will, C. M. 2004, *ApJ*, 611, 1080